Unified coupled-mode theory for geometric and material perturbations in optical waveguides

Gianluca Guerra, Seyed Mohammad Abokhamis Mousavi, Austin Taranta, Eric Numkam Fokoua *Member, IEEE*, Marco Santagiustina *Member, IEEE*, Andrea Galtarossa *Fellow, IEEE*, Francesco Poletti *Senior Member, IEEE*, and Luca Palmieri *Member, IEEE*

***Abstract*—Coupled-mode theory is a powerful tool to understand and control the effects of deployment and fabrication imperfections on optical waveguides. Although it provides many advantages compared to the finite element method, it still lacks the ability to treat geometric and material perturbations when they act simultaneously on the waveguide. This work fills this gap, providing a novel framework for a unified treatment of geometric and material perturbations in the coupled-mode analysis. The proposed approach consists of, first, applying the theory of transformation optics to convert geometric deformation into material perturbations and, second, studying the obtained waveguide by using a custom-developed coupled-mode theory able to deal with perturbations of both the permittivity and the permeability tensor.**

The framework is applied to three examples: a solid-core fiber affected by intrinsic perturbations, a bent solid-core fiber, and an elliptical hollow-core fiber. Results are validated against simulations based on the finite element method and compared with the standard coupled-mode theory most suitable for each specific example; they show that the proposed unified coupled-mode theory performs consistently better than standard theories, confirming it as a general and accurate tool for the design and analysis of optical waveguides.

***Index Terms*—Coupled-mode theory, perturbations, deformations, transformation optics, optical waveguides.**

I. Introduction

ELECTROMAGNETIC waveguides underpin a vast array of technologies that are crucial to modern life, from microwave antennae, to the global optical fiber telecommunications infrastructure, to cutting-edge integrated photonic circuits. With the development of increasingly advanced systems, the properties of the electromagnetic (EM) waves traversing the waveguides must be understood and controlled at an exceptional level of detail. This is especially true in optical systems, like space-division multiplexing transmission and resonant devices [1], [2], where the waveguides must be designed and fabricated with a precision better than fractions of the wavelength of light. To this end, waveguide designers will usually devise symmetric and translationally invariant waveguides because, in these simple waveguides, they can easily find modes that decompose light into its constituent parts [3], [4]. These modes can be found from the waveguide cross-section by using, for example, finite element method (FEM) solvers [5]–[7].

In practice, however, the waveguide differs from the designed one because of imperfect fabrication and environmental perturbations, both of which can vary randomly and uncontrollably along it. As a result, light may propagate unpredictably, jeopardizing the functioning of the system [8]. The brute force approach to study perturbed waveguides would consist in numerically solving the complete three-dimensional EM problem. Nevertheless, this task requires in general considerable computational resources and, even worse, does not provide clear physical insight on the propagation properties of the waveguide.

A much more effective approach to the study of perturbed waveguide is the coupled-mode theory (CMT) [9]–[11]. CMT expands the EM wave propagating in the waveguide of interest as a linear combination of modes derived from a reference waveguide. More specifically, the coefficients of the linear combination, i.e., the complex amplitudes of the modes, are free to vary along the longitudinal coordinate to accommodate for variations of the actual waveguide with respect to the reference one. Powerful as it is, CMT does not have a unique comprehensive formulation, but it is typically specialized for specific classes of waveguides and perturbations. The main reason preventing a unified approach is the intimate difference between material and geometric perturbations. Actually, material perturbations modify the waveguide's dielectric permittivity tensors, whereas geometric perturbations (or deformations) change the waveguide's domains and structure and hence the boundary conditions of the EM problem. Owing to this conceptual difference, theoreticians have formulated CMTs that work with either material perturbations [10], [12]–[16] or specific geometric deformations [17], [18]; yet, a single theory able to treat both cases simultaneously is still lacking.

Gianluca Guerra is with the Optoelectronics Research Centre, University of Southampton, Highfield Campus, Southampton, SO17 1BJ, United Kingdom, and with the Department of Information Engineering, University of Padova, 35131 Padova, Italy (email: g.guerra@soton.ac.uk).

Seyed Mohammad Abokhamis Mousavi, Austin Taranta, Eric Numkam Fokoua, and Francesco Poletti are with the Optoelectronics Research Centre, University of Southampton, Highfield Campus, Southampton, SO17 1BJ, United Kingdom.

Marco Santagiustina, Andrea Galtarossa, and Luca Palmieri are with the Department of Information Engineering, University of Padova, 35131 Padova, Italy (email: luca.palmieri@unipd.it).

This work is partly supported by MIUR—Italian Ministry for Education, University and Research—as part of the "Departments of Excellence" initiative (law 232/2016) and from PRIN 2017 project Fiber Infrastructure for Research on Space-division multiplexed Transmission (FIRST); from the University of Padova BIRD 2019 project MACFIBER; and from the ERC project Lightpipe (grant No. 682724).

Manuscript received April 19, 2021; revised August 16, 2021.

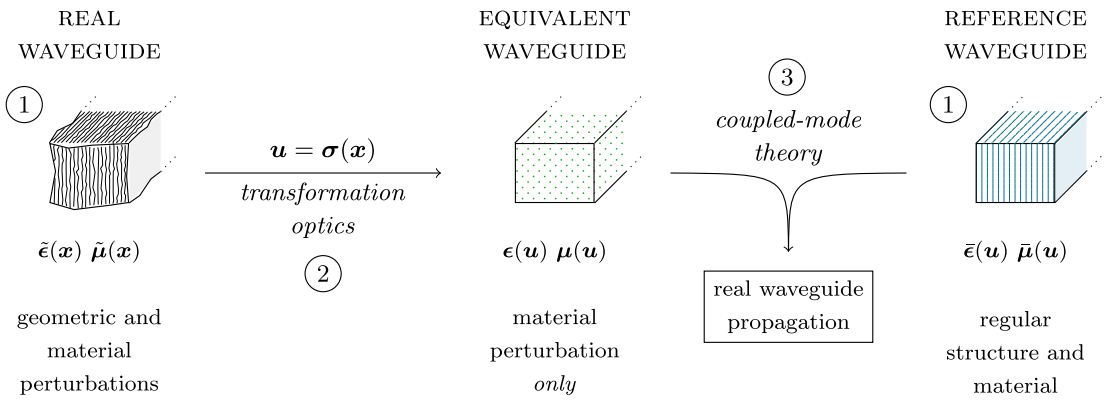

Fig. 1. Schematic representation of the UCMT. (1) The real waveguide has arbitrary geometry and material, while the reference waveguide has regular geometry and material and supports modes. When compared to the reference, the real waveguide has both geometric and material perturbations. (2) Using transformation optics, the real waveguide is transformed into an electromagnetically equivalent one with the same geometry of the reference; this results in further material perturbations. (3) A specific coupled-mode theory for material perturbations is used to describe the equivalent waveguide in terms of coupling between the modes of the reference waveguide.

A possible workaround to this problem consists in modeling geometric deformations as the difference between the constitutive tensors of the real waveguide and the reference one, treating deformations as material perturbations [19]–[21]. This workaround, however, can hardly be implemented in waveguides with thin and complex structures, such as photonic crystals or microstructured fibers. More critically, it fails to properly consider how deformations change the boundary conditions of the EM field, resulting in poor accuracy [22].

In this work, expanding our preliminary theory presented in Ref. [23], we present a CMT formulation that works independently of the type of perturbation affecting the waveguide, unifying the treatment of geometric and material perturbations. Whatever the perturbations are, geometric, material, or geometric and material simultaneously, the proposed *unified coupled-mode theory* (UCMT) handles them exactly, without the need of workarounds that compromise the accuracy. The proposed formulation uses the theory of transformation optics (TO) to convert geometric deformations into material perturbations [24], [25], thus treating in the exact way the change in the boundary conditions. The use of TO, however, induces both perturbations on the permittivity and the permeability tensor, a condition not considered by standard CMTs for material perturbations; therefore, we developed a novel theory to handle this specific case. The resulting UCMT works seamlessly with TO and supports anisotropy and both guided and leaky modes.

The remainder of this paper is organized as follows. In Section II, we present the formulation of the UCMT. In Section III, we demonstrate its capability by reporting examples of use, validating the results against FEM. Finally, in Section IV, we conclude our work by summarizing the obtained results.

II. The unified coupled-mode theory

The proposed UCMT is based on the formulation schematically illustrated in Fig. 1; it takes in consideration three waveguides: the real, the equivalent, and the reference waveguide. The *real waveguide* is the one under study, represented with respect to the coordinate system $\boldsymbol{x} = (x, y, z)$ and described by its dielectric permittivity tensor $\tilde{\boldsymbol{\epsilon}}(\boldsymbol{x})$ and magnetic permeability tensor $\tilde{\boldsymbol{\mu}}(\boldsymbol{x})$. The *reference waveguide* is the one used as reference for the UCMT, where its modes are employed to describe the propagation within the real waveguide. To be suitable for the UCMT, the reference waveguide should support modes, which means that it must be translationally invariant (or periodic), and must be reciprocal [4]. The reference waveguide is represented in the most suitable coordinate system $\boldsymbol{u} = (u, v, s)$ and is described by its constitutive tensors $\bar{\boldsymbol{\epsilon}}(\boldsymbol{u})$ and $\bar{\boldsymbol{\mu}}(\boldsymbol{u})$ (note the bars used here and the tildes used for the tensors of the real waveguide). When compared to the reference, the real waveguide is usually affected by both material and geometric perturbations. Finally, the *equivalent waveguide* is obtained by using TO to transform the geometry of the real waveguide into that of the reference one. This is achieved by a proper coordinate transformation $\boldsymbol{u} = \boldsymbol{\sigma}(\boldsymbol{x})$ and, according to TO, it results in a new set of constitutive tensors $\boldsymbol{\epsilon}(\boldsymbol{u})$ and $\boldsymbol{\mu}(\boldsymbol{u})$. In this way, the equivalent waveguide describes *exactly* both the geometry and the material properties of the real waveguide while having the same geometry of the reference one.

Once the three waveguides are defined, the propagation in the equivalent waveguide can be expressed as a linear combination of the modes of the reference one. Nevertheless, the application of TO leads in general to anisotropic constitutive tensors; in particular, the fact that the magnetic one, $\boldsymbol{\mu}(\boldsymbol{u})$, might be non-constant and anisotropic requires special care, as this eventuality has never been considered in previous CMTs. There are a few different approaches in which the coupling coefficients, i.e., the coefficients of the linear combination, can be calculated leading to the actual CMT. Since we want the UCMT to be able to describe the guiding properties, including losses, we implement it using both the guided and the leaky modes of the reference waveguide. As shown below, this gives enough flexibility to precisely model both lossless and lossy waveguides. A consequence of this choice is that the reference waveguide must be reciprocal, to guarantee orthogonality relations for both leaky and guided modes (we discuss this aspect in Section II-B). Reciprocal

waveguides are those with symmetric constitutive tensors [26], and they comprise almost every class of waveguides with the only exception of very exotic ones, such as those subjected to strong magnetic fields or made of magnetized plasmonic media [27]. We remark, however, that reciprocity is required only for the reference waveguide and not for the real one.

A. Definition of the equivalent waveguide

The equivalent waveguide is obtained by mapping the real one through a proper coordinate transformation, so that, in the new coordinate system, its geometry is equal to that of the reference waveguide. We achieve this using the theory of TO, which allows one to write Maxwell's equations with respect to a transformed space [28]. For the details about TO we defer the reader to the cited literature; here we just recall the main results. Let $\{\tilde{\mathbf{E}}, \tilde{\mathbf{H}}\}$ be the EM field in a volume with constitutive tensors $\tilde{\boldsymbol{\epsilon}}$ and $\tilde{\boldsymbol{\mu}}$, expressed with respect to the coordinate system $\boldsymbol{x} = (x, y, z)$. Let $\boldsymbol{u} = \boldsymbol{\sigma}(\boldsymbol{x})$ be a transformation from the coordinate system $\boldsymbol{x}$ to a new system $\boldsymbol{u} = (u, v, s)$, and let $\boldsymbol{J}_{\boldsymbol{\sigma}}$ be the associated Jacobian matrix. According to TO, with respect to the coordinate system $\boldsymbol{u}$, the following fields

$$\mathbf{E}(\boldsymbol{u}) = \boldsymbol{J}_{\boldsymbol{\sigma}}^{-\top} \tilde{\mathbf{E}}(\boldsymbol{\sigma}^{-1}(\boldsymbol{u})), \tag{1a}$$

$$\mathbf{H}(\boldsymbol{u}) = \boldsymbol{J}_{\boldsymbol{\sigma}}^{-\top} \tilde{\mathbf{H}}(\boldsymbol{\sigma}^{-1}(\boldsymbol{u})), \tag{1b}$$

satisfy Maxwell's equations with constitutive tensors [25], [29]

$$\boldsymbol{\epsilon}(\boldsymbol{u}) = (\det \boldsymbol{J}_{\boldsymbol{\sigma}})^{-1} \boldsymbol{J}_{\boldsymbol{\sigma}} \, \tilde{\boldsymbol{\epsilon}} \, \boldsymbol{J}_{\boldsymbol{\sigma}}^{\top}, \tag{2a}$$

$$\boldsymbol{\mu}(\boldsymbol{u}) = (\det \boldsymbol{J}_{\boldsymbol{\sigma}})^{-1} \boldsymbol{J}_{\boldsymbol{\sigma}} \, \tilde{\boldsymbol{\mu}} \, \boldsymbol{J}_{\boldsymbol{\sigma}}^{\top}, \tag{2b}$$

where the superscript $^{-1}$ indicates inversion and superscript $^{\top}$ indicates transposition. Effectively, TO takes the space of the real waveguide and, by deforming it, maps the waveguide geometry into a new coordinate system where the waveguide's structure is the same as the reference. This transformation converts any geometrical difference between the real and the reference waveguide into a material perturbation embedded into the equivalent one. Consequently, the resulting material perturbation of the equivalent waveguide is a representation of both the material and the geometric perturbation of the real one.

B. The coupling coefficients

The UCMT describes how light propagates through the equivalent waveguide by using linear combinations of the modes of the reference waveguide. The mathematical derivation of the corresponding coefficients is rather cumbersome and is detailed in the appendix; here, we report only the main findings.

For convenience, we formulate the theory *à la* Marcuse [10]. In particular, we describe the equivalent and the reference waveguide in the same coordinate space $\boldsymbol{u} = (u, v, s)$, to which we associate the Cartesian reference frame $\{\hat{\mathbf{u}}, \hat{\mathbf{v}}, \hat{\mathbf{s}}\}$, with $\hat{\mathbf{s}} = (0, 0, 1)^{\top}$ pointing at the direction of propagation. This choice avoids using intricate curvilinear formulations of Maxwell's equations [17]. We decompose the constitutive tensor $\boldsymbol{\epsilon}$ as $\boldsymbol{\epsilon} = \boldsymbol{\epsilon}_{tt} + \boldsymbol{\epsilon}_{ts} + \boldsymbol{\epsilon}_{st} + \boldsymbol{\epsilon}_{ss}$, where $\boldsymbol{\epsilon}_{tt}$, $\boldsymbol{\epsilon}_{ts}$ and $\boldsymbol{\epsilon}_{st}$ read

$$\begin{pmatrix} \epsilon_{uu} & \epsilon_{uv} & 0 \\ \epsilon_{vu} & \epsilon_{vv} & 0 \\ 0 & 0 & 0 \end{pmatrix}, \begin{pmatrix} 0 & 0 & \epsilon_{us} \\ 0 & 0 & \epsilon_{vs} \\ 0 & 0 & 0 \end{pmatrix}, \begin{pmatrix} 0 & 0 & 0 \\ 0 & 0 & 0 \\ \epsilon_{su} & \epsilon_{sv} & 0 \end{pmatrix}, \tag{3}$$

respectively, and the only non-zero element of $\boldsymbol{\epsilon}_{ss}$ is ϵ_{ss} in position $(3, 3)$. Similar decompositions are applied to all the other involved tensors. Regarding the modes, we denote them by using Greek letters, and we indicate their propagating direction by using superscripts surrounded by parenthesis, e.g., $\nu^{(p)}$ identifies the mode ν propagating towards p, where p can be either forward $(+)$ or backward $(-)$. We indicate the complex amplitudes of the modes as $a_{\nu}^{(p)}(s)$. As common to any CMT, the dependence on s of these amplitudes is described by a set of linear differential equations, which are more conveniently expressed in vector notation, leading to the *coupled-mode equation* [12]

$$\frac{\mathrm{d}\boldsymbol{a}}{\mathrm{d}s} = -j \left[\mathbf{D} + \mathbf{X}(s)\right] \boldsymbol{a}(s), \tag{4}$$

where $\mathbf{D}$ is the constant diagonal matrix of the (possibly complex) mode propagation constants, and $\mathbf{X}(s)$ is the coupling matrix whose elements are the coupling coefficients. Matrix $\mathbf{D}$ describes how the modes propagate in the reference waveguide, whereas $\mathbf{X}(s)$, the coupling matrix, describes the local coupling (or interactions) that occurs among the modes in the equivalent waveguide because of the perturbations. The explicit expression of $\mathbf{X}(s)$ depends on the specific way in which the CMT has been formulated; therefore, it represents the most interesting and distinctive aspect of each CMT.

As noted, our approach requires the development of a new CMT able to deal with both permittivity and permeability perturbations. Following the common approach, we use the superposition principle to describe the combined effect of both perturbations as the sum of the effects that each perturbation would have if it were acting alone, which is correct up to a first order of approximation. Therefore, the matrix $\mathbf{X}(s)$ is expressed as

$$\mathbf{X}(s) = -\mathbf{Q} \left(\mathbf{K}(s) + \mathbf{C}(s)\right), \tag{5}$$

where the matrices $\mathbf{K}(s)$ and $\mathbf{C}(s)$ account for the permittivity and the permeability perturbation, respectively. The constant matrix $\mathbf{Q}$ is related only to the orthogonality of the modes of the reference waveguide and hence does not depend on the perturbations. Considering two generic modes $\xi^{(q)}$ and $\nu^{(p)}$, the corresponding elements of $\mathbf{K}(s)$ are given by

$$K_{\xi,\nu}^{(q,p)}(s) = \omega \iint \left(\mathbf{T}\, \mathbf{e}_{\xi}^{(q)}\right)^{\top} \mathbf{M}(s) \left(\mathbf{T}\, \mathbf{e}_{\nu}^{(p)}\right) \mathrm{d}A, \tag{6}$$

where $\mathbf{e}$ is the electric field of the indicated mode, ω is the angular frequency, $\mathbf{T}$ and $\mathbf{M}(s)$ are 3×3 matrices, and the integration is extended to the entire waveguide cross-section. $\mathbf{T}$ is a function of the reference waveguide's dielectric profile $\bar{\boldsymbol{\epsilon}}$ (thus is independent of s) and is given by

$$\mathbf{T} = \mathbf{I}_3 + \frac{\bar{\boldsymbol{\epsilon}}_{st}}{\bar{\epsilon}_{ss}}, \tag{7}$$

where $\mathbf{I}_3$ is the 3×3 identity matrix. $\mathbf{M}(s)$ is a function of both $\bar{\boldsymbol{\epsilon}}$ and the equivalent waveguide's dielectric profile $\boldsymbol{\epsilon}$

given by Eq. (2a), which may depend on s according to the perturbations; its exact expression reads

$$\mathbf{M}(s) = \boldsymbol{\epsilon}_{tt} - (\bar{\boldsymbol{\epsilon}} - \bar{\boldsymbol{\epsilon}}_{ss}) + \frac{\bar{\epsilon}_{ss}}{\epsilon_{ss}} (\boldsymbol{\epsilon} - \boldsymbol{\epsilon}_{tt} - \bar{\boldsymbol{\epsilon}}_{ss}) - \left(\frac{\boldsymbol{\epsilon}_{ts}\, \boldsymbol{\epsilon}_{st}}{\epsilon_{ss}} - \frac{\bar{\boldsymbol{\epsilon}}_{ts}\, \bar{\boldsymbol{\epsilon}}_{st}}{\bar{\epsilon}_{ss}} \right). \quad (8)$$

Regarding matrix $\mathbf{C}(s)$, similar expressions hold for its coefficients, but this time they involve the magnetic field $\mathbf{h}$ and the permeability tensors $\bar{\boldsymbol{\mu}}$ and $\boldsymbol{\mu}$ of the waveguides. The exact expressions can be calculated using the duality theorem for EM fields [26], and they read

$$C_{\xi,\nu}^{(q,p)}(s) = -\omega \iint \left(\mathbf{S}\, \mathbf{h}_{\xi}^{(q)} \right)^{\top} \mathbf{N}(s) \left(\mathbf{S}\, \mathbf{h}_{\nu}^{(p)} \right) \mathrm{d}A, \quad (9)$$

where

$$\mathbf{S} = \mathbf{I}_3 + \frac{\bar{\boldsymbol{\mu}}_{st}}{\bar{\mu}_{ss}}, \quad (10)$$

and

$$\mathbf{N}(s) = \boldsymbol{\mu}_{tt} - (\bar{\boldsymbol{\mu}} - \bar{\boldsymbol{\mu}}_{ss}) + \frac{\bar{\mu}_{ss}}{\mu_{ss}} (\boldsymbol{\mu} - \boldsymbol{\mu}_{tt} - \bar{\boldsymbol{\mu}}_{ss}) - \left(\frac{\boldsymbol{\mu}_{ts}\, \boldsymbol{\mu}_{st}}{\mu_{ss}} - \frac{\bar{\boldsymbol{\mu}}_{ts}\, \bar{\boldsymbol{\mu}}_{st}}{\bar{\mu}_{ss}} \right). \quad (11)$$

As shown by Eqs. (6) and (9), the expressions of the coupling coefficients are, as typical for CMTs, overlap integrals involving the two coupled modes and quantities related to the perturbations. In general, the complete formulas are quite cumbersome, but for small perturbations they simplify to (see App. B for details):

$$K_{\xi,\nu}^{(q,p)}(s) \approx \omega \iint \mathbf{e}_{\xi}^{(q)\top}\, (\boldsymbol{\epsilon} - \bar{\boldsymbol{\epsilon}})\, \mathbf{e}_{\nu}^{(p)}\, \mathrm{d}A, \quad (12)$$

$$C_{\xi,\nu}^{(q,p)}(s) \approx -\omega \iint \mathbf{h}_{\xi}^{(q)\top}\, (\boldsymbol{\mu} - \bar{\boldsymbol{\mu}})\, \mathbf{h}_{\nu}^{(p)}\, \mathrm{d}A, \quad (13)$$

which have the typical form of overlap integrals between the modes fields and the perturbation more commonly encountered in the literature [20], [30].

Matrix $\mathbf{Q}$ contains the *orthogonality coefficients* that describe the relations of orthogonality among the modes. In reciprocal waveguides, the coefficients are either ± 1 for non-orthogonal or 0 for orthogonal modes [31], [32]:

$$Q_{\xi,\nu}^{(q,p)} = \begin{cases} 1 & \text{if } \nu = \xi,\ (q) = (+),\ (p) = (-) \\ -1 & \text{if } \nu = \xi,\ (q) = (-),\ (p) = (+) \\ 0 & \text{otherwise} \end{cases}. \quad (14)$$

In other words, $Q_{\xi,\nu}^{(q,p)}$ is not zero if and only if ν and ξ are the same modes but counter-propagating, which also means that forward- and backward-propagating modes form a bi-orthonormal basis [15], [16]. As a consequence, when a mode is considered in the UCMT, also its counter-propagating one needs to be considered, even though the designer may only be interested in forward propagation.

For a generic CMT to be exact, the coupled-mode equation should consider a complete basis of modes. Among them, there is the continuum of radiation modes [3]. In our theory, however, we consider leaky modes instead of the radiation ones. We avoid considering radiation modes because the continuous spectrum makes them harder to find and use. Besides, radiation modes do not belong to real-life waveguides, where the cross-section is finitely extended and the external coating dampens any wave that radiates out. When such a coating is modelled as a perfectly matched layer (PML) [33], the radiating modes become leaky [34]. Therefore, leaky modes approximate the radiation ones near the core of the waveguide—the most important region for the guiding properties—but they form a discrete set so they are easier to find and use.

Guided and leaky modes form an infinite set; however, practical implementation of the CMT will only consider a finite subset of it, sacrificing accuracy for feasibility. How many and which modes should be considered is arguably one of the most important practical aspects. Yet a systematic rule does not exist and, as the next examples show, the number of modes required depends on their type, the waveguides, and the perturbations being considered.

III. Validation and Examples

In this section we validate the UCMT by studying three waveguides of practical interest, namely: a strongly guiding solid-core fiber affected by stress anisotropy and core ellipticity; a bent, weakly guiding solid-core fiber; and an elliptically deformed hollow-core fiber. We choose these cases because the corresponding equivalent waveguides are translationally invariant, so they support modes that can be numerically calculated using a commercial FEM solver [35]. In this way, we can assess the accuracy of the UCMT by comparing the propagation constants calculated numerically with those obtained by the UCMT. In the framework of the UCMT, the modes of the equivalent waveguide are expressed as linear combinations of those of the reference waveguide. Given that modes propagate independently of each other, the actual modes of the equivalent waveguide can be found in terms of those of the reference by diagonalizing matrix $\mathbf{D} + \mathbf{X}$, and their propagation constants are the eigenvalues of $\mathbf{D} + \mathbf{X}$.

Note that this comparison with the numerical solutions can be done because the chosen models are translationally invariant and hence the matrix $\mathbf{X}$ is constant. Nevertheless, we remark that the framework is not restricted to translationally invariant waveguides alone, but it can be applied also to longitudinally varying ones.

For clarity, hereinafter we call *eigenmodes* the modes of the equivalent waveguide, whereas we continue calling *modes* those of the reference one. All the following numerical examples are evaluated at 1550 nm wavelength.

A. Strongly guiding fiber affected by intrinsic perturbations

As a first example, we consider a strongly guiding structure affected by both geometric and material perturbations; namely, an air-clad fiber affected by core ellipticity and stress-induced anisotropy. These two perturbations are the most common ones encountered in optical fibers, as they naturally arise during the drawing process [36]. In the framework of the UCMT, the real waveguide is the actual one affected by stress-induced anisotropy and ellipticity, while we choose the ideal, isotropic, circularly-symmetric fiber as reference waveguide. As illustrated in Fig. 2, the equivalent waveguide is obtained

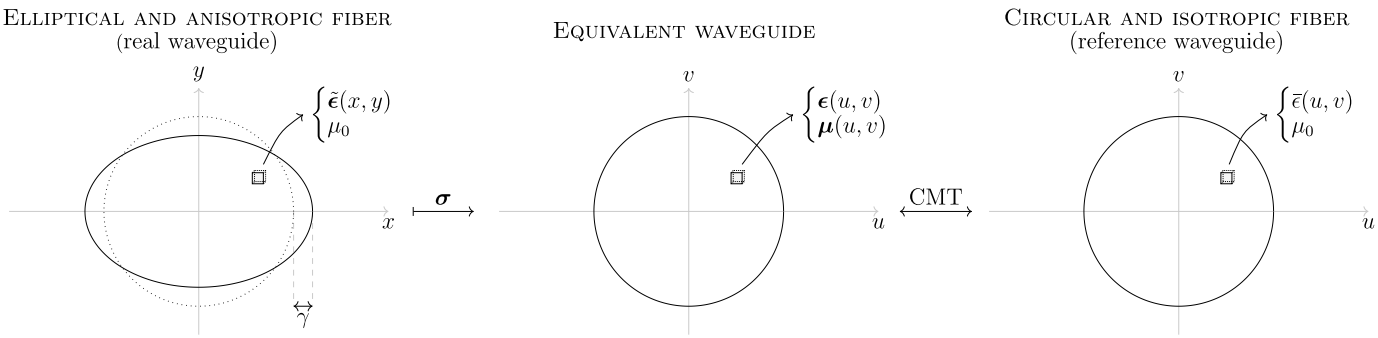

Fig. 2. Application of the UCMT to the example. (left) the elliptical and anisotropic fiber under study; (center) the equivalent waveguide is computed, using TO, from the coordinate transformation $\boldsymbol{\sigma}$ that recovers the circular shape; (right) the circular and isotropic ideal fiber is used as reference in the CMT.

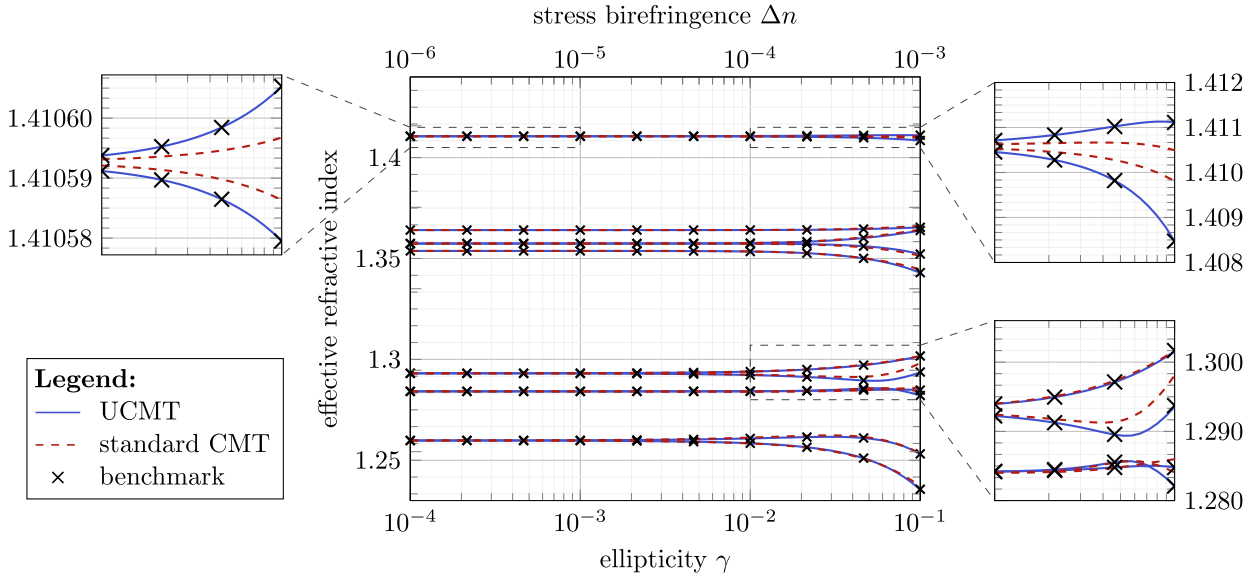

Fig. 3. Effective refractive index of the first twelve guided eigenmodes of an air-cladded fiber with elliptical and birefringent core. Results are computed both by using the UCMT proposed in this paper (blue curves) and the standard CMT for guided-modes [10] (red-dashed curves), and are compared with FEM results ($\times$ marks).

by applying to the real waveguide the transformation that makes it circular.

We model the anisotropy as bi-axial and parametrized by the difference Δn between the two axes of birefringence—Δn is zero outside the silica core. When the anisotropy is aligned to the u- and to the v-axis, the dielectric tensor becomes [20]

$$\boldsymbol{\epsilon}_{\text{sa}}(u,v) = \begin{pmatrix} \bar{\epsilon} + \frac{\Delta\epsilon}{2} & 0 & 0 \\ 0 & \bar{\epsilon} - \frac{\Delta\epsilon}{2} & 0 \\ 0 & 0 & \bar{\epsilon} \end{pmatrix}, \tag{15}$$

where $\Delta\epsilon \approx 2\epsilon_0 \bar{n}\,\Delta n$, $\bar{\epsilon}(u,v) = \epsilon_0\,\bar{n}^2(u,v)$, and $\bar{n}(u,v)$ is the refractive index profile of the ideal fiber. Regarding the ellipticity, it deforms the fiber structure from circular to elliptical, shifting any point of coordinate (u,v) to (x,y) according to

$$\begin{aligned} x(u,v) &= (1+\gamma)\,u, \\ y(u,v) &= (1-\gamma)\,v, \end{aligned} \tag{16}$$

where both (u,v) and (x,y) are Cartesian coordinates, and γ is the maximum relative shift that occurs along the axes of the elliptical deformation. As defined in Eq. (16), these axes are aligned with those of the material anisotropy in Eq. (15). This choice is reasonable since in telecom optical fibers the anisotropy and the ellipticity are both caused by the thermal mismatch [30], [37].

We obtain the elliptical and anisotropic fiber under study (real waveguide) by combining the two perturbations and by applying them, simultaneously, to the reference waveguide. From Eqs. (15) and (16), its dielectric tensor reads

$$\tilde{\boldsymbol{\epsilon}}(x,y) = \boldsymbol{\epsilon}_{\text{sa}}\left(\frac{x}{1+\gamma}, \frac{y}{1-\gamma}\right). \tag{17}$$

From this fiber, we get the equivalent waveguide by applying the coordinate transformation $(u,v,s) = \boldsymbol{\sigma}(x,y,z)$ that undoes the ellipticity and recovers the ideal circular structure: this transformation is simply the inverse of Eq. (16) with $s = z$, and its Jacobian matrix reads

$$\boldsymbol{J}_{\boldsymbol{\sigma}} = \begin{pmatrix} 1/(1+\gamma) & 0 & 0 \\ 0 & 1/(1-\gamma) & 0 \\ 0 & 0 & 1 \end{pmatrix}. \tag{18}$$

Then, according to Eqs. (2), the permittivity and permeability

tensors of the equivalent waveguide are

$$\boldsymbol{\epsilon} = \begin{pmatrix} \frac{1-\gamma}{1+\gamma}\left(\bar{\epsilon}+\frac{\Delta\epsilon}{2}\right) & 0 & 0 \\ 0 & \frac{1+\gamma}{1-\gamma}\left(\bar{\epsilon}-\frac{\Delta\epsilon}{2}\right) & 0 \\ 0 & 0 & \left(1-\gamma^2\right)\bar{\epsilon} \end{pmatrix}, \quad \boldsymbol{\mu} = \begin{pmatrix} \frac{1-\gamma}{1+\gamma} & 0 & 0 \\ 0 & \frac{1+\gamma}{1-\gamma} & 0 \\ 0 & 0 & 1-\gamma^2 \end{pmatrix} \mu_0. \tag{19}$$

As a numerical example, we choose the ideal air-cladded fiber (reference waveguide) with core refractive index $n_{\text{co}} = 1.444$ and core radius $r_{\text{co}} = 1.75\,\mu$m; at 1550 nm, it propagates 30 guided modes. We fix the ratio between γ and Δn such that $\gamma/\Delta n = 100$ and we span typical values of γ in the range $[10^{-4},\ 10^{-1}]$. With this ratio, the two perturbations contribute the same amount of modal birefringence to the fundamental mode, which is typical of telecom single-mode fibers [36].

Fig. 3 shows the propagation constants in terms of effective refractive index of the first twelve guided eigenmodes. Solid blue lines are the results obtained with our UCMT, while black cross marks are those obtained with the FEM solver that we use as benchmark. For all the values of perturbation, our theory is precise and performs very close to the benchmark, as shown in the three zoomed insets. Remarkably, as shown in the top-left inset, the UCMT also accurately computes the perturbation-induced modal birefringence between otherwise degenerate modes; for example, when $\gamma = 10^{-3}$ and $\Delta n = 10^{-5}$, the ellipticity and anisotropy combined induce a birefringence on the fundamental mode of the order of $\sim 10^{-5}$ that our theory estimates with an absolute error of $\sim 10^{-8}$.

Besides benchmarking our UCMT against FEM, we also compare it against the standard CMT for anisotropic waveguides and guided modes [10]. As customary, in the standard CMT the ellipticity of the core is modelled simply as the difference between the refractive index profile of the elliptical fiber and that of the reference one [19]. The result is represented by dashed red lines in Fig. 3. Although the standard CMT provides a correct qualitative behavior, it is not as accurate as the UCMT, which consistently performs closer to the benchmark.

B. Bent weakly guiding fiber

In this example, we look at bending effects on a step-index single-mode fiber. As the fiber bends, its structure material becomes anisotropic via the elasto-optic effect. Both the deformation and the anisotropy affect the propagation, resulting in the electromagnetic field being pushed outward from the core and in the direction opposite that of the bending [38]. The modeling is slightly more complicated than the preceding example because two reference frames are required (see Fig. 4): the first one, $\{\hat{\mathbf{x}}, \hat{\mathbf{y}}, \hat{\mathbf{z}}\}$, is fixed with respect to the laboratory, while the second one, $\{\hat{\mathbf{u}}, \hat{\mathbf{v}}, \hat{\mathbf{s}}\}$, is local and follows the fiber bend. We assume also that the axes $\hat{\mathbf{y}}$ and $\hat{\mathbf{v}}$ (which are parallel) are orthogonal to the curvature plane where the fiber lays. The relationship between the coordinate spaces (x, y, z) and (u, v, s) of the two reference frames is given by [39]:

$$\begin{aligned} x(u,v,s) &= -R_b + (R_b+u)\cos(s/R_b), \\ y(u,v,s) &= v, \\ z(u,v,s) &= (R_b+u)\sin(s/R_b). \end{aligned} \tag{20}$$

As the fiber bends, a complex strain field builds up in it, but only two directional components of this strain significantly affect light propagation [40]. The main one occurs along the longitudinal axis $\hat{\mathbf{s}}$ and is due to the outer ($u > 0$) material being stretched and the inner one ($u < 0$) being compressed. The secondary one occurs along the bending direction $-\hat{\mathbf{u}}$ and is due to the pressure exerted by the outer material onto the inner one. Both effects stress the fiber materials, making them anisotropic. Expressed in the local frame, the dielectric tensor of the bent fiber reads [20]

$$\tilde{\boldsymbol{\epsilon}}(u,v) = \bar{\epsilon}\,\mathbf{I}_3 - \frac{u}{R_b}\frac{\bar{\epsilon}^2}{\epsilon_0}\begin{pmatrix} q_1 & 0 & 0 \\ 0 & q_2 & 0 \\ 0 & 0 & q_2 \end{pmatrix} + \frac{r_{cl}^2}{2R_b^2}\frac{\bar{\epsilon}^2}{\epsilon_0}\begin{pmatrix} q_2 & 0 & 0 \\ 0 & q_1 & 0 \\ 0 & 0 & q_1 \end{pmatrix}, \tag{21}$$

where $q_1 = 0.206$, $q_2 = 0.032$ are elasto-optic coefficients for silica glass, and r_{cl} is the fiber cladding radius. The first term is the dielectric profile that the fiber would have if it were not bent. The second and third terms are due to the stresses along $\hat{\mathbf{s}}$ and $-\hat{\mathbf{u}}$, respectively. Before applying TO to obtain the equivalent waveguide, the dielectric tensor must be expressed with respect to the laboratory frame; this is achieved by the transformation $\boldsymbol{R}_y^\top\,\tilde{\boldsymbol{\epsilon}}\,\boldsymbol{R}_y$, where $\boldsymbol{R}_y$ is the rotation matrix

$$\boldsymbol{R}_y(s) = \begin{pmatrix} \cos(s/R_b) & 0 & \sin(s/R_b) \\ 0 & 1 & 0 \\ -\sin(s/R_b) & 0 & \cos(s/R_b) \end{pmatrix}. \tag{22}$$

Owing to the general expressions (2), the constitutive tensors of the equivalent waveguide can now be calculated as

$$\begin{aligned} \boldsymbol{\epsilon}(u,v) &= (\det \boldsymbol{J}_{\boldsymbol{\sigma}})^{-1}\,\boldsymbol{J}_{\boldsymbol{\sigma}}\,\boldsymbol{R}_y^\top\,\tilde{\boldsymbol{\epsilon}}\,\boldsymbol{R}_y\,\boldsymbol{J}_{\boldsymbol{\sigma}}^\top, \\ \boldsymbol{\mu}(u,v) &= (\det \boldsymbol{J}_{\boldsymbol{\sigma}})^{-1}\,\boldsymbol{J}_{\boldsymbol{\sigma}}\,\boldsymbol{J}_{\boldsymbol{\sigma}}^\top\,\mu_0, \end{aligned} \tag{23}$$

where the Jacobian matrix $\boldsymbol{J}_{\boldsymbol{\sigma}}$ is the inverse of the Jacobian matrix of (20), and can be factorized as:

$$\boldsymbol{J}_{\boldsymbol{\sigma}}(u,v,s) = \begin{pmatrix} 1 & 0 & 0 \\ 0 & 1 & 0 \\ 0 & 0 & R_b/(R_b+u) \end{pmatrix}\boldsymbol{R}_y. \tag{24}$$

Explicit calculations easily confirm that the constitutive tensors are independent of s, i.e., the equivalent waveguide is translational invariant, similarly to what happens in case of twist [41]. Note also, that if the stress on the material is neglected, i.e., if $\tilde{\boldsymbol{\epsilon}} = \bar{\epsilon}\,\mathbf{I}_3$, then the result of (23) coincides with that reported in Ref. [39] about the geometric effect of bending on a hollow-core Bragg fiber.

Having defined the equivalent waveguide, we study the propagation using the UCMT. The reference fiber is a straight, isotropic and single-mode step-index fiber, which supports only a pair of degenerate guided modes. These have circular

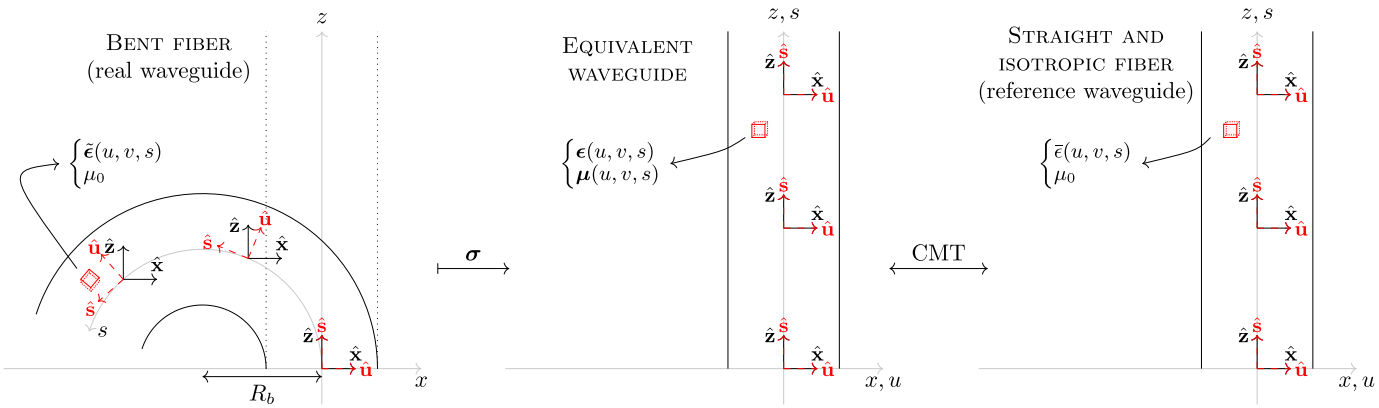

Fig. 4. Schematic representation of the bend fiber. (left) the fiber is bent with bending radius R_b, and its dielectric tensor changes accordingly with the stress induced on the material; (center) the equivalent waveguide is computed from the coordinate transformation $\boldsymbol{\sigma}$ that straightens the bend; (right) the straight and isotropic fiber is used as reference in the UCMT.

symmetry, therefore any coupling between them result in a circularly symmetric field, which cannot correctly describe the shift of the field towards the outside of the bend, actually observed in a bent fiber. To overcome this issue, leaky modes must be considered, too; in the following analysis we considered 200 modes, two of which guided and the others leaky.

As an example, we assume the reference fiber with core radius of $r_{co} = 4.5\,\mu$m, cladding radius $r_{cl} = 100\,\mu$m, and with core and cladding refractive indices of $n_{co} = 1.448$ and $n_{cl} = 1.444$, respectively. Since we also consider the leaky modes, we surround the fiber's cross-section with a PML. We bend the fiber with a radius that spans from 2 cm to 25 cm, and we look at the propagation constants of its two most guided eigenmodes.

The results are shown in Fig. 5(a), where we plot the effective refractive indices of the two most guided eigenmodes for three different cases, namely considering only geometric deformation (dashed, blue curves), only elasto-optic stress (dashed, yellow curves) and both effects simultaneously (solid, red curves). Interestingly, the geometric deformation has a much larger impact on the propagation constants than the elasto-optic stress; moreover, when acting together the two effects tend to slightly mitigate each other. From the graph, it is also evident that, as expected, bending breaks the degeneracy of the modes, giving rise to birefringence. The induced modal birefringence (difference between the refractive indices of the two orthogonally polarized modes) is plotted in Fig. 5(b). We note that the effect of the geometric deformation is largely negligible with respect to the effect of the elasto-optic stress, which is practically the only source of modal birefringence. In all cases the results of the UCMT are in very good agreement to the FEM simulations, represented by black crosses. The error in terms of effective refractive index is always less than 2.5×10^{-7}, a value reached for the tightest bend ($R_b = 2$ cm) when both deformation and stress are considered. In this example we do not report the comparison with standard CMT just because that theory cannot be used to model simultaneously geometrical and stress effects induced by bending.

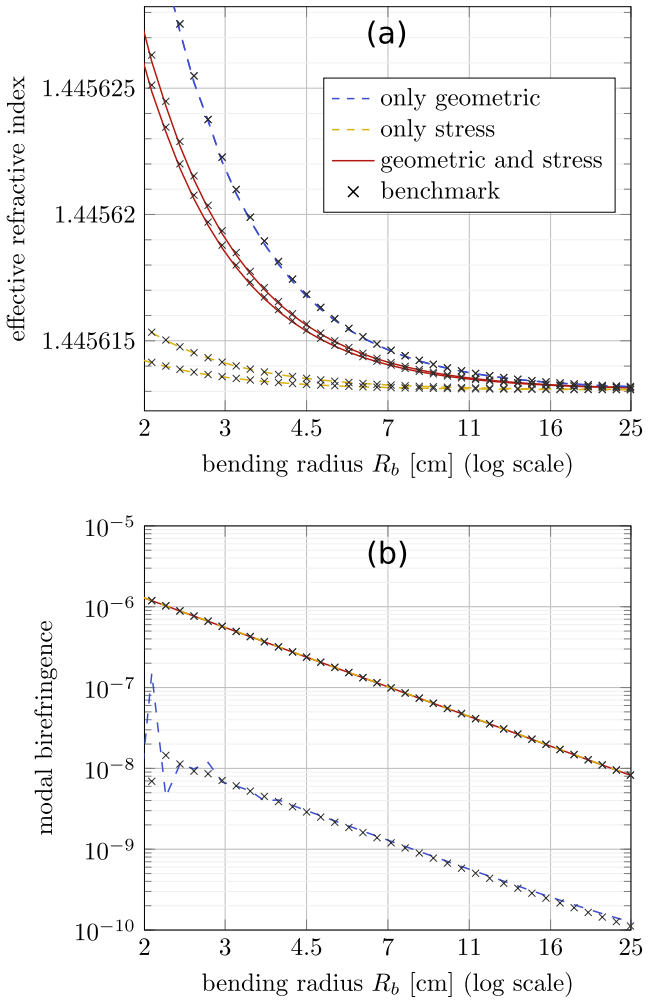

Fig. 5. Analysis of a bent single-mode fiber performed with the proposed UCMT and compared with the numerical benchmark (× marks) for three different cases—only geometric deformation (dashed, blue curves), only elasto-optic stress (dashed, yellow curves), and both of them simultaneously (solid, red curves). (a) Effective refractive index of the two most guided eigenmodes and (b) the corresponding modal birefringence.

C. Hollow-core fiber affected by ellipticity

A hollow-core fiber consists of a cladding structure made of glass and a core made of air where light propagates. Since light is confined in the air, these fibers could bring many of the advantages of free-space propagation [42]–[44]. Although a great deal of effort in hollow-core fiber development is directed toward decreasing attenuation, the extent to which fiber imperfections affect this parameter has seen little investigation. In this example we show how our theory can be used for this purpose.

We consider the simplest hollow-core fiber, made of a circular air hole in a bulk of glass [45], and we study it when the hole is slightly elliptical. This specific example is chosen to highlight the ability of the UCMT to analyze also waveguides where propagation is supported by leaky modes.

We select as reference waveguide the ideal circular hollow-core fiber, with core radius $r_{\text{co}} = 30\,\mu m$, and refractive indices $n_{\text{co}} = 1$ (air core) and $n_{\text{cl}} = 1.444$ (silica glass cladding). In the numerical model the fiber is surrounded by a PML placed beyond $75\,\mu m$ from the fiber axis. At $1550\,\text{nm}$, we use the 30 lowest-loss leaky modes of the reference to study the eigenmodes of the equivalent waveguide. The ellipticity is modeled as in Eq. (16), where γ is varied between 10^{-4} and 10^{-1}.

Results are reported in Fig. 6, which shows the propagation constants of the twelve lowest-loss eigenmodes of the fiber for different values of core ellipticity γ. Specifically, Fig. 6(a) shows the real part of the propagation constants expressed in terms of effective refractive index, while Fig. 6(b) shows their imaginary part expressed in terms of loss in dB/m. Solid blue lines indicate the results obtained with our UCMT and black crosses are the benchmark values from FEM simulations. The dashed red lines are the results obtained with the standard CMT for leaky modes proposed in Ref. [14] where, as in Sec. III-A, the ellipticity is modelled as the difference between the dielectric permittivity of the circular fiber and the elliptical one.

Results from our theory are in excellent agreement with the benchmark, especially at low and medium values of γ. It is slightly less accurate when the ellipticity is strong, although this is only appreciable by looking at the loss. The reason is that a loss of $1\,\text{dB}/\text{m}$ corresponds to an effective refractive index imaginary part of $\simeq -2.5 \times 10^{-8}$ at $1550\,\text{nm}$, so loss requires in general high precision to be estimated. At $\gamma = 10^{-1}$, the UCMT estimates the effective refractive index of the highest-loss eigenmode with an absolute error of $\sim 10^{-6}$ on both the real and the imaginary part.

The UCMT performs much better than the standard CMT, which does not follow the correct behavior when the ellipticity is medium or large. As already discussed in Sec. III-A, the lack of accuracy of the standard CMT is due to its inability to correctly model the geometrical change of the boundary conditions. This has drastic effects in leaky waveguides, because the leakier is the eigenmode, the closer its EM field is to the core-cladding boundary, and the more sensitive it is to changes in the boundary conditions. As a result, the performance of the standard CMT worsens when eigenmodes have high losses. For this reason, a CMT treating geometric perturbations would have been a more equitable point of comparison against our UCMT for this example. Nevertheless, these CMTs are available only for lossless waveguides, and although one example has been adapted to study a bent hollow-core fiber [39], it is specialized and valid only for that particular case and not suitable for generic deformations.

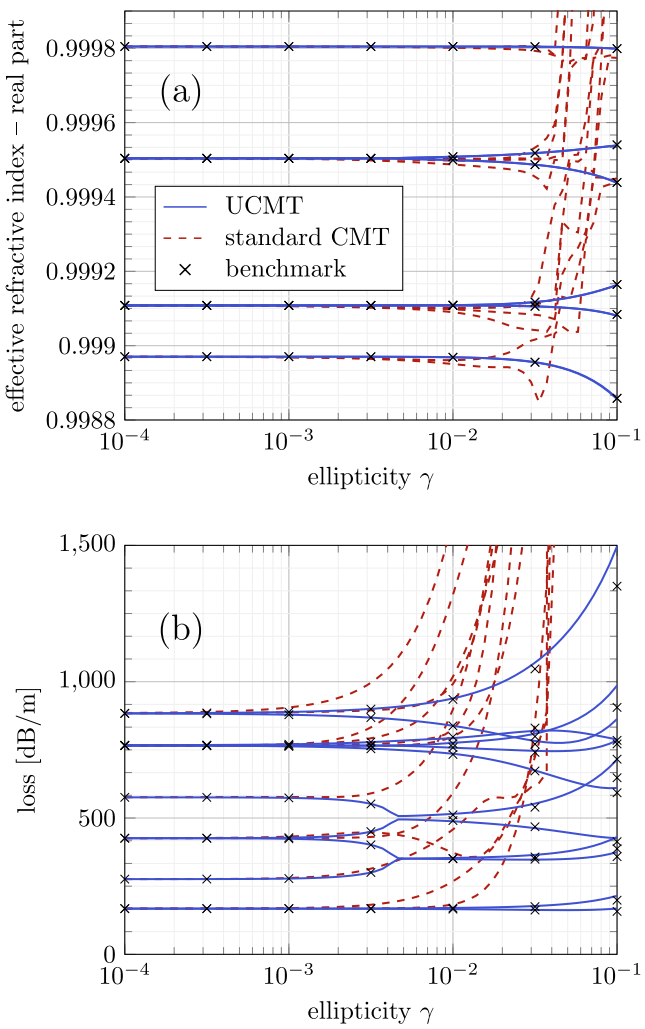

Fig. 6. Analysis of an elliptical hollow-core fiber. Real part of effective refractive index (a) and losses (b) of the twelve lowest-loss leaky eigenmodes. Blue curves are the results of the proposed UCMT; dashed, red curves are obtained with the standard CMT described in Ref. [14]; × marks are the numerical benchmark.

IV. Conclusion

In this work we proposed a unified coupled-mode theory (UCMT) to study optical waveguides when they are affected by both geometric and material perturbations simultaneously, a common scenario previously impossible to be investigated with standard coupled-mode theories. The proposed UCMT uses the theory of transformation optics (TO) to convert geometric deformations into material perturbations, and an *ad hoc* developed coupled-mode theory to deal with both dielectric and magnetic perturbations, and with both guided and leaky modes.

We validated our UCMT in three key cases, showing that in every case it performs very close to FEM simulations, proving that it can accurately track different aspects of the propagation, including propagation constants, modal birefringence, and losses. As with any CMT, the UCMT may require a variable number of modes to obtain accurate results. However, the number of modes required to achieve a given level of accuracy is not easily predictable and it depends on the type of modes, waveguides, and perturbations. In the analyzed examples we have observed that the scenario requiring more modes is that which considers both leaky and guided modes. Since leaky modes are close together and far from the guided ones in terms of propagation constants, they tend to couple among themselves before coupling with the others. As a consequence, many leaky modes must be considered to evaluate their effects on the guiding properties.

Accuracy is also affected by the size of the perturbations: for a fixed number of modes it decreases as the perturbations become larger. Indeed, the larger the perturbations, the more the waveguide deviates from the reference, so more modes are required to compensate for the deviation and achieve a target accuracy. Ideally, one would always use all the modes including leaky ones, but since these are infinite in number, one must compromise between accuracy and the numerical complexity, which scales with the square of the number of modes. It is worthwhile remarking, however, that since these modes are those of the reference waveguide, they must be calculated only once; afterwards, they can be used for any kind of perturbation, as long as the reference waveguide is not changed.

Besides FEM simulations, when possible we have compared the UCMT against the standard CMTs that one would conventionally use to study propagation in optical waveguides. In the considered cases, UCMT performed always better than CMTs, actually outperforming them for strong perturbations. The advantage of UCMT with respect to standard CMTs lies in its ability to properly treat properly geometric deformations and the corresponding changes in the boundary conditions of the associated EM problem. By contrast, standard CMTs treat these deformations simply as the difference between the dielectric profile of the real waveguide and the reference one, resulting in a poor description of the EM fields and a general drop of accuracy. Moreover, this approach is not viable when the deformations are not limited to the cross-section, like in the case of bending.

The theory which we present here can be a powerful new tool in the waveguide designer's arsenal. It can be applied to a wide range of waveguides, from standard solid-core fibers, to multi-core fibers, to waveguides with more complex cladding structures such as nested antiresonant nodeless hollow-core fibers [43]. Indeed, although we have shown only introductory examples to validate the UCMT, there are no limitations on the nature of the perturbations that a waveguide designer can study. They only need to describe the waveguide as a mapping from their chosen reference waveguide and have its modes available. The mapping can include irregular features of the waveguide's structure, like a defect localized in a specific area of the cross-section. When dealing with many of these irregularities, the waveguide designer may construct the mapping as a superposition of localized transformations, each targeting a specific feature. Moreover, UCMT allows a designer to study perturbations whose magnitudes evolve, possibly randomly, along the waveguide's direction of propagation, as it is often the case with twist and micro-bending in drawn fibers. The coupled-mode equation describes how the coupling occurs at a given *local* length. Hence, computing the coupling matrix $\mathbf{X}(s)$ and integrating the coupled-mode equation along the waveguide is enough for the designer to study the propagation.

The flexibility and accuracy over conventional approaches render the UCMT ideal for the typical waveguide design process in which structures are optimized for a particular performance parameter. Moreover, it can be used to study situations where finite element methods are intractable or time-intensive, for example, in helping to understand waveguides' operating range or to design waveguides robust to specific perturbations or manufacturing variations.

APPENDIX A
DERIVATION OF THE COUPLED-MODE THEORY

In this section, we derive the proposed UCMT following the procedure outlined by Marcuse in his CMT [10]. We start by reducing Maxwell's equations to a set of equations for the transverse components of the field. The electromagnetic fields $\mathbf{E}(u,v,s)$ and $\mathbf{H}(u,v,s)$ solve Maxwell's equations in the harmonic regime [26]:

$$\boldsymbol{\nabla} \times \mathbf{H} = j\omega \boldsymbol{\epsilon}\, \mathbf{E}, \tag{25a}$$

$$\boldsymbol{\nabla} \times \mathbf{E} = -j\omega \boldsymbol{\mu}\, \mathbf{H}, \tag{25b}$$

where ω is the angular frequency, $\boldsymbol{\epsilon}(u,v,s)$ and $\boldsymbol{\mu}(u,v,s)$ are the permittivity and the permeability tensor of the waveguide. Without loss of generality, we decompose the fields as $\mathbf{E} = \mathbf{E}_t + \mathbf{E}_s$ and $\mathbf{H} = \mathbf{H}_t + \mathbf{H}_s$, where hereinafter subscripts t and s indicate the transverse and longitudinal components, respectively. Similarly, we can decompose the nabla operator as $\boldsymbol{\nabla} = \boldsymbol{\nabla}_t + \hat{\mathbf{s}}\,\partial/\partial s$. As a result, Maxwell's equations are split into their transverse and longitudinal terms. Namely, the transverse ones are:

$$\nabla_t \times \mathbf{H}_s + \hat{\mathbf{s}} \times \frac{\partial \mathbf{H}_t}{\partial s} = j\omega \left(\boldsymbol{\epsilon}_{tt}\, \mathbf{E}_t + \boldsymbol{\epsilon}_{ts}\, \mathbf{E}_s\right), \tag{26a}$$

$$\nabla_t \times \mathbf{E}_s + \hat{\mathbf{s}} \times \frac{\partial \mathbf{E}_t}{\partial s} = -j\omega \left(\boldsymbol{\mu}_{tt}\, \mathbf{H}_t + \boldsymbol{\mu}_{ts}\, \mathbf{H}_s\right), \tag{26b}$$

while the longitudinal ones read:

$$\mathbf{E}_s = -j\frac{1}{\omega}\frac{1}{\epsilon_{ss}} \nabla_t \times \mathbf{H}_t - \frac{1}{\epsilon_{ss}} \boldsymbol{\epsilon}_{st}\, \mathbf{E}_t, \tag{27a}$$

$$\mathbf{H}_s = j\frac{1}{\omega}\frac{1}{\mu_{ss}} \nabla_t \times \mathbf{E}_t - \frac{1}{\mu_{ss}} \boldsymbol{\mu}_{st}\, \mathbf{H}_t, \tag{27b}$$

where we used $\boldsymbol{\epsilon}_{ss}\, \mathbf{E}_s = \epsilon_{ss}\, \mathbf{E}_s$ and $\boldsymbol{\mu}_{ss}\, \mathbf{H}_s = \mu_{ss}\, \mathbf{H}_s$. Finally, by substituting Eq. (27) into (26), we obtain:

$$\begin{aligned} \nabla_t \times \Big[-\frac{\nabla_t \times \mathbf{E}_t}{j\omega\mu_{ss}} - \frac{\boldsymbol{\mu}_{st}}{\mu_{ss}}\, \mathbf{H}_t \Big] + \hat{\mathbf{s}} \times \frac{\partial \mathbf{H}_t}{\partial s} = \\ j\omega \boldsymbol{\epsilon}_{tt}\, \mathbf{E}_t + \frac{\boldsymbol{\epsilon}_{tz}}{\epsilon_{ss}}\, \nabla_t \times \mathbf{H}_t - j\omega \frac{\boldsymbol{\epsilon}_{ts}\, \boldsymbol{\epsilon}_{st}}{\epsilon_{ss}}\, \mathbf{E}_t, \end{aligned} \tag{28a}$$

$$\sum_{\nu,p}\Big(\frac{\mathrm{d}a_\nu^{(p)}}{\mathrm{d}s}+j\gamma_\nu^{(p)}a_\nu^{(p)}\Big)(\hat{\mathbf{s}}\times\mathbf{h}_{\nu t}^{(p)})=\sum_{\nu,p}a_\nu^{(p)}\Big\{j\omega\Big[(\boldsymbol{\epsilon}_{tt}-\bar{\boldsymbol{\epsilon}}_{tt})-\Big(\frac{\boldsymbol{\epsilon}_{ts}\boldsymbol{\epsilon}_{st}}{\epsilon_{ss}}-\frac{\bar{\boldsymbol{\epsilon}}_{ts}\bar{\boldsymbol{\epsilon}}_{st}}{\bar{\epsilon}_{ss}}\Big)\Big]\mathbf{e}_{\nu t}^{(p)}+\Big(\frac{\boldsymbol{\epsilon}_{ts}}{\epsilon_{ss}}-\frac{\bar{\boldsymbol{\epsilon}}_{ts}}{\bar{\epsilon}_{ss}}\Big)\nabla_t\times\mathbf{h}_{\nu t}^{(p)}\Big\},\quad(30a)$$

$$\sum_{\nu,p}\Big(\frac{\mathrm{d}a_\nu^{(p)}}{\mathrm{d}s}+j\gamma_\nu^{(p)}a_\nu^{(p)}\Big)(\hat{\mathbf{s}}\times\mathbf{e}_{\nu t}^{(p)})=\sum_{\nu,p}a_\nu^{(p)}\,\nabla_t\times\Big[-\frac{1}{j\omega}\Big(\frac{1}{\epsilon_{ss}}-\frac{1}{\bar{\epsilon}_{ss}}\Big)\nabla_t\times\mathbf{h}_{\nu t}^{(p)}+\Big(\frac{\boldsymbol{\epsilon}_{st}}{\epsilon_{ss}}-\frac{\bar{\boldsymbol{\epsilon}}_{st}}{\bar{\epsilon}_{ss}}\Big)\mathbf{e}_{\nu t}^{(p)}\Big].\quad(30b)$$

$$\nabla_t\times\Big[\frac{\nabla_t\times\mathbf{H}_t}{j\omega\epsilon_{ss}}-\frac{\boldsymbol{\epsilon}_{st}}{\epsilon_{ss}}\mathbf{E}_t\Big]+\hat{\mathbf{s}}\times\frac{\partial\mathbf{E}_t}{\partial s}=-j\omega\boldsymbol{\mu}_{tt}\mathbf{H}_t+\frac{\boldsymbol{\mu}_{ts}}{\mu_{ss}}\nabla_t\times\mathbf{E}_t+j\omega\frac{\boldsymbol{\mu}_{ts}\boldsymbol{\mu}_{st}}{\mu_{ss}}\mathbf{H}_t,\quad(28b)$$

where the only unknowns are the transverse fields $\mathbf{E}_t$ and $\mathbf{H}_t$. Since Eqs. (27) express the longitudinal field $\mathbf{E}_s$ and $\mathbf{H}_s$ in terms of the transverse one, solving (28) is enough to determine the entire field.

Following the standard approach of any CMT, the fields are expressed as a longitudinally varying linear combination of the modes of the reference waveguide, that is:

$$\mathbf{E}_t(u,v,s)=\sum_{\nu,p}a_\nu^{(p)}(s)\,\mathbf{e}_{\nu t}^{(p)}(u,v),\quad(29a)$$

$$\mathbf{H}_t(u,v,s)=\sum_{\nu,p}a_\nu^{(p)}(s)\,\mathbf{h}_{\nu t}^{(p)}(u,v),\quad(29b)$$

where $\mathbf{e}_{\nu t}^{(p)}$ and $\mathbf{h}_{\nu t}^{(p)}$ are the transverse field of the mode $\nu^{(p)}$, p indicates the mode direction of propagation, $a_\nu^{(p)}$ is the mode complex amplitude, and the sum is extended to all the modes of the reference waveguide, either forward- or backward-propagating, guided or leaky. When the mode $\nu^{(p)}$ propagates within the reference waveguide, the full electromagnetic field is $\boldsymbol{\mathcal{E}}_\nu^{(p)}(u,v,s)=\mathbf{e}_\nu^{(p)}(u,v)\exp(-j\gamma_\nu^{(p)}s)$ and $\boldsymbol{\mathcal{H}}_\nu^{(p)}(u,v,s)=\mathbf{h}_\nu^{(p)}(u,v)\exp(-j\gamma_\nu^{(p)}s)$, where $\gamma_\nu^{(p)}$ is the propagation constant. For future use, it is worthwhile to note that these fields solve all the above equations once the constitutive tensors $\boldsymbol{\epsilon}$ and $\boldsymbol{\mu}$ are substituted for the ones of the reference waveguide $\bar{\boldsymbol{\epsilon}}$ and $\bar{\boldsymbol{\mu}}$. In particular, this is true in (27) and (28), once we substitute $\mathbf{E}_t$ and $\mathbf{E}_s$ with $\boldsymbol{\mathcal{E}}_{\nu t}^{(p)}$ and $\boldsymbol{\mathcal{E}}_{\nu s}^{(p)}$, respectively, and make analogous substitution for the magnetic fields.

Perturbation of the permittivity tensor

In order to proceed, we start by assuming that only the permittivity tensor is perturbed, that is, $\boldsymbol{\epsilon}(u,v,s)\neq\bar{\boldsymbol{\epsilon}}(u,v)$ and $\boldsymbol{\mu}(u,v,s)=\bar{\boldsymbol{\mu}}(u,v)$. By inserting Eqs. (29) into (28), and combining the result with (28) rephrased in terms of $\mathbf{e}_{\nu t}^{(p)}$ and $\mathbf{h}_{\nu t}^{(p)}$, we obtain Eqs. (30), reported at the top of this page. Now we pre-multiply both sides of (30) by the transverse fields, sum the two equations and integrate the result over the waveguide cross-section; more specifically, we evaluate the quantity

$$\iint\Big[\mathbf{e}_{\xi t}^{(q)\top}\cdot(30\mathrm{a})+\mathbf{h}_{\xi t}^{(q)\top}\cdot(30\mathrm{b})\Big]\,\mathrm{d}A,\quad(31)$$

whose expansion yields Eq. (32) reported at the top of the next page. Both the left-hand side and the right-hand side of (32) can be further manipulated. Regarding the left-hand side, we apply the vector identity $(\mathbf{a}\times\mathbf{b})\times\mathbf{c}=(\mathbf{a}\cdot\mathbf{c})\,\mathbf{b}-(\mathbf{b}\cdot\mathbf{c})\,\mathbf{a}$, to obtain

$$\sum_{\nu,p}Q_{\xi,\nu}^{(q,p)}\Big(\frac{\mathrm{d}a_\nu^{(p)}}{\mathrm{d}s}+j\gamma_\nu^{(p)}a_\nu^{(p)}\Big),\quad(33)$$

where the coefficients $Q_{\xi,\nu}^{(q,p)}$ are

$$Q_{\xi,\nu}^{(q,p)}=\iint\hat{\mathbf{s}}\cdot\Big[\mathbf{e}_\xi^{(q)}\times\mathbf{h}_\nu^{(p)}-\mathbf{e}_\nu^{(p)}\times\mathbf{h}_\xi^{(q)}\Big]\,\mathrm{d}A.\quad(34)$$

These coefficients describe the orthogonality between the modes of the reference waveguide and do not depend on the perturbation. In the special, yet very common, case that the reference waveguide is reciprocal, using the reciprocity theorem [26] and by properly normalizing the modes, it can be proved that the coefficients $Q_{\xi,\nu}^{(q,p)}$ read as in (14) [31], [32].

Regarding the right-hand side of (32), we start from its last term under integration, to which we apply the vector identity $\mathbf{a}^\top(\nabla\times\mathbf{b})=(\nabla\times\mathbf{a})^\top\mathbf{b}-\nabla\cdot(\mathbf{a}\times\mathbf{b})$ to obtain

$$(\nabla_t\times\mathbf{h}_{\xi t}^{(q)})^\top\Big[-\frac{1}{j\omega}\Big(\frac{1}{\epsilon_{ss}}-\frac{1}{\bar{\epsilon}_{ss}}\Big)\nabla_t\times\mathbf{h}_{\nu t}^{(p)}+\Big(\frac{\boldsymbol{\epsilon}_{st}}{\epsilon_{ss}}-\frac{\bar{\boldsymbol{\epsilon}}_{st}}{\bar{\epsilon}_{ss}}\Big)\mathbf{e}_{\nu t}^{(p)}\Big]-\nabla_t\cdot\Big\{\mathbf{h}_{\xi t}^{(q)}\times\Big[-\frac{1}{j\omega}\Big(\frac{1}{\epsilon_{ss}}-\frac{1}{\bar{\epsilon}_{ss}}\Big)\nabla_t\times\mathbf{h}_{\nu t}^{(p)}+\Big(\frac{\boldsymbol{\epsilon}_{st}}{\epsilon_{ss}}-\frac{\bar{\boldsymbol{\epsilon}}_{st}}{\bar{\epsilon}_{ss}}\Big)\mathbf{e}_{\nu t}^{(p)}\Big]\Big\}.\quad(35)$$

When (35) is integrated over the entire fiber cross-section, the divergence term yields zero. This can be proved by applying the two-dimensional divergence theorem and noting that the equivalent line integral along the waveguide cross-section contour tends to zero because the mode fields tend to zero away from the waveguide axis. Moreover, when (27) is evaluated for the modes of the reference waveguide, we readily find $\nabla_t\times\mathbf{h}_{\xi t}^{(q)}=j\,\omega\,(\bar{\boldsymbol{\epsilon}}_{st}\,\mathbf{e}_{\xi t}^{(q)}+\bar{\epsilon}_{ss}\,\mathbf{e}_{\xi s}^{(q)})$, and hence the double integral on the right-hand side of (32) can be rearranged as in Eq. (36) at the bottom of the next page. Finally, (36) can be written in a more compact form, such as

$$-j\sum_{\nu,p}K_{\xi,\nu}^{(q,p)}(s)\,a_\nu^{(p)}(s),\quad(37)$$

where the coupling coefficients $K_{\xi,\nu}^{(q,p)}(s)$ are given in (6). Putting back together the two sides of the equation, we obtain the scalar coupled-mode equation for dielectric perturbations

$$\sum_{\nu,p}Q_{\xi,\nu}^{(q,p)}\Big(\frac{\mathrm{d}a_\nu^{(p)}}{\mathrm{d}s}+j\gamma_\nu^{(p)}a_\nu^{(p)}\Big)=-j\sum_{\nu,p}K_{\xi,\nu}^{(q,p)}\,a_\nu^{(p)}.\quad(38)$$

$$\sum_{\nu,p}\Big(\frac{\mathrm{d}a_\nu^{(p)}}{\mathrm{d}s}+j\gamma_\nu^{(p)}a_\nu^{(p)}\Big)\iint-\Big[\mathbf{e}_{\xi t}^{(q)\top}\left(\hat{\mathbf{s}}\times\mathbf{h}_{\nu t}^{(p)}\right)+\mathbf{h}_{\xi t}^{(q)\top}\left(\hat{\mathbf{s}}\times\mathbf{e}_{\nu t}^{(p)}\right)\Big]\,\mathrm{d}A=$$
$$-\sum_{\nu,p}a_\nu^{(p)}\iint\Big\{j\omega\,\mathbf{e}_{\xi t}^{(q)\top}\left(\boldsymbol{\epsilon}_{tt}-\bar{\boldsymbol{\epsilon}}_{tt}\right)\mathbf{e}_{\nu t}^{(p)}+\mathbf{e}_{\xi t}^{(q)\top}\left(\frac{\boldsymbol{\epsilon}_{ts}}{\epsilon_{ss}}-\frac{\bar{\boldsymbol{\epsilon}}_{ts}}{\bar{\epsilon}_{ss}}\right)\nabla_t\times\mathbf{h}_{\nu t}^{(p)}-j\omega\,\mathbf{e}_{\xi t}^{(q)\top}\left(\frac{\boldsymbol{\epsilon}_{ts}\,\boldsymbol{\epsilon}_{st}}{\epsilon_{ss}}-\frac{\bar{\boldsymbol{\epsilon}}_{ts}\,\bar{\boldsymbol{\epsilon}}_{st}}{\bar{\epsilon}_{ss}}\right)\mathbf{e}_{\nu t}^{(p)}$$
$$+\mathbf{h}_{\xi t}^{(q)\top}\nabla_t\times\Big[-\frac{1}{j\omega}\Big(\frac{1}{\epsilon_{ss}}-\frac{1}{\bar{\epsilon}_{ss}}\Big)\nabla_t\times\mathbf{h}_{\nu t}^{(p)}+\Big(\frac{\boldsymbol{\epsilon}_{st}}{\epsilon_{ss}}-\frac{\bar{\boldsymbol{\epsilon}}_{st}}{\bar{\epsilon}_{ss}}\Big)\mathbf{e}_{\nu t}^{(p)}\Big]\Big\}\mathrm{d}A \quad (32)$$

Perturbation of the permeability tensor

In principle, to derive the scalar coupled-mode equation for a perturbation of the permeability tensor, we could repeat the above analysis with respect to the magnetic field. In practice, it is much more straightforward and elegant to apply the duality theorem of EM fields [26]. Assuming that sources and free charges are both zero, this theorem states that if $\{\mathbf{E},\mathbf{H}\}$ is the EM field in a volume with constitutive tensors $\boldsymbol{\epsilon}$ and $\boldsymbol{\mu}$, then the field $\{\mathbf{E}',\mathbf{H}'\}$ is a valid solution of Maxwell's equations in a volume with constitutive tensors $\boldsymbol{\epsilon}'$ and $\boldsymbol{\mu}'$, provided that the following substitutions are performed

$$\mathbf{E}'=-\mathbf{H},\quad \mathbf{H}'=\mathbf{E},\quad \boldsymbol{\epsilon}'=\boldsymbol{\mu},\quad \boldsymbol{\mu}'=\boldsymbol{\epsilon}; \quad (39)$$

$\{\mathbf{E}',\mathbf{H}'\}$ is called the dual field. According to the theorem, a magnetic perturbation on $\boldsymbol{\mu}$ corresponds to a dielectric perturbation on $\boldsymbol{\epsilon}'$, which can be studied with the theory described in the previous sections. To begin with, note that owing to (39), the modes of the dual field have the same propagation constants $\gamma_\nu^{(p)}$; similarly, applying (39) to (29) we see that the dual field has also the same modes amplitudes $a_\nu^{(p)}(s)$. Therefore, the scalar coupled-mode equation for the dual field reads as in (38), with the coefficients $Q_{\xi,\nu}^{(q,p)}$ and $K_{\xi,\nu}^{(q,p)}$ substituted by the corresponding dual ones $K_{\xi,\nu}^{\prime(q,p)}(s)$ and $Q_{\xi,\nu}^{\prime(q,p)}(s)$; these are defined as in (6) and (34) but for the dual field $\{\mathbf{E}',\mathbf{H}'\}$. If we now apply the substitutions (39), we find that $Q_{\xi,\nu}^{\prime(q,p)}(s)=-Q_{\xi,\nu}^{(q,p)}(s)$ and $K_{\xi,\nu}^{\prime(q,p)}(s)=-C_{\xi,\nu}^{(q,p)}(s)$, as defined in (9). In conclusion the scalar coupled-mode equation for a magnetic perturbation can be expressed as

$$\sum_{\nu,p}Q_{\xi,\nu}^{(q,p)}\Big(\frac{\mathrm{d}a_\nu^{(p)}}{\mathrm{d}s}+j\gamma_\nu^{(p)}a_\nu^{(p)}\Big)=-j\sum_{\nu,p}C_{\xi,\nu}^{(q,p)}\,a_\nu^{(p)}. \quad (40)$$

Simultaneous perturbation of the constitutive tensors

To the best of our knowledge, the above theoretical treatment does not lead to general closed form expressions when the perturbation is applied on both the constitutive tensors. However, this case can be studied by applying the superposition principle, according to which the coupling that occurs when both constitutive tensors are perturbed is equal to the sum of the coupling occurring when each of them is perturbed independently of the other. Mathematically this corresponds to stating that the coupling coefficients are the sum of $K_{\xi,\nu}^{(q,p)}$ and $C_{\xi,\nu}^{(q,p)}$; accordingly, the coupled-mode equation reads

$$\sum_{\nu,p}Q_{\xi,\nu}^{(q,p)}\Big(\frac{\mathrm{d}a_\nu^{(p)}}{\mathrm{d}s}+j\gamma_\nu^{(p)}a_\nu^{(p)}\Big)=$$
$$-j\sum_{\nu,p}\Big(K_{\xi,\nu}^{(q,p)}(s)+C_{\xi,\nu}^{(q,p)}(s)\Big)\,a_\nu^{(p)}. \quad (41)$$

We observe that this approach is correct up to the first order of approximation because it does not account for the coupling due to the mutual change of permittivity and permeability, which are second order or higher effects. Note that this is what is customarily done in standard CMTs, where the coupling originated by several perturbations is described as the sum of the coupling due to each perturbation as if it were acting alone.

The vector coupled-mode equation

The scalar coupled-mode equation (41) is written for each mode considered in the analysis, leading to a system of equations. It is convenient to represent this system in vector notation, reaching the vector coupled-mode equation

$$\mathbf{Q}\left(\frac{\mathrm{d}\boldsymbol{a}}{\mathrm{d}s}+j\,\mathbf{D}\,\boldsymbol{a}\right)=-j\,\left(\mathbf{K}(s)+\mathbf{C}(s)\right)\,\boldsymbol{a}, \quad (42)$$

where $\boldsymbol{a}(s)$ is the vector of the modes' amplitudes; $\mathbf{Q}$ is the orthogonality matrix, whose elements are the mode orthogonality coefficients $Q_{\xi,\nu}^{(q,p)}$; $\mathbf{D}$ is the diagonal matrix of the modes' propagation constants $\gamma_\nu^{(p)}$; and $\mathbf{K}(s)$ and $\mathbf{C}(s)$ are the matrices of the coefficients $K_{\xi,\nu}^{(q,p)}(s)$ and $C_{\xi,\nu}^{(q,p)}(s)$. Owing to the linear independece of the modes, $\mathbf{Q}$ is invertible and the coupled-mode equation can be rearranged as

$$\frac{\mathrm{d}\boldsymbol{a}}{\mathrm{d}s}=-j\left[\mathbf{D}+\mathbf{X}(s)\right]\boldsymbol{a}(s), \quad (43)$$

where

$$\mathbf{X}(s)=\mathbf{Q}^{-1}\left(\mathbf{K}(s)+\mathbf{C}(s)\right). \quad (44)$$

$$-j\omega\sum_{\nu,p}a_\nu^{(p)}\iint\Big\{\mathbf{e}_{\xi t}^{(q)\top}\Big[\left(\boldsymbol{\epsilon}_{tt}-\bar{\boldsymbol{\epsilon}}_{tt}\right)-\Big(\frac{\boldsymbol{\epsilon}_{ts}\,\boldsymbol{\epsilon}_{st}}{\epsilon_{ss}}-\frac{\bar{\boldsymbol{\epsilon}}_{ts}\,\bar{\boldsymbol{\epsilon}}_{st}}{\bar{\epsilon}_{ss}}\Big)\Big]\mathbf{e}_{\nu t}^{(p)}+\mathbf{e}_{\xi t}^{(q)\top}\Big(\frac{\bar{\epsilon}_{ss}}{\epsilon_{ss}}\boldsymbol{\epsilon}_{ts}-\bar{\boldsymbol{\epsilon}}_{ts}\Big)\Big(\frac{\bar{\boldsymbol{\epsilon}}_{st}}{\bar{\epsilon}_{ss}}\,\mathbf{e}_{\nu t}^{(p)}+\mathbf{e}_{\nu s}^{(p)}\Big)$$
$$-\Big(\frac{\bar{\boldsymbol{\epsilon}}_{st}}{\bar{\epsilon}_{ss}}\,\mathbf{e}_{\xi t}^{(q)}+\mathbf{e}_{\xi s}^{(q)}\Big)^{\top}\Big[\bar{\epsilon}_{ss}\Big(\frac{\bar{\epsilon}_{ss}}{\epsilon_{ss}}-1\Big)\Big(\frac{\bar{\boldsymbol{\epsilon}}_{st}}{\bar{\epsilon}_{ss}}\,\mathbf{e}_{\nu t}^{(p)}+\mathbf{e}_{\nu s}^{(p)}\Big)-\Big(\frac{\bar{\epsilon}_{ss}}{\epsilon_{ss}}\boldsymbol{\epsilon}_{st}-\bar{\boldsymbol{\epsilon}}_{st}\Big)\mathbf{e}_{\nu t}^{(p)}\Big]\Big\}\,\mathrm{d}A, \quad (36)$$

This expression of the coupled-mode equation is the most general one and also applies to the (rather uncommon) case in which the reference waveguide is selected to be non-reciprocal. As already noted, in the more common case in which the reference waveguide is reciprocal, the coefficients $Q_{\xi,\nu}^{(q,p)}$ read as in (14); then, it can be shown that $\mathbf{Q}^{-1} = -\mathbf{Q}$, leading to Eq. (5).

APPENDIX B
SIMPLIFIED COUPLING COEFFICIENTS

In this section we derived simplified expressions for the coefficients $K_{\xi,\nu}^{(q,p)}$ and $C_{\xi,\nu}^{(q,p)}$ in a few cases of interest.

Given that the choice of the reference waveguide is to a large extent arbitrary, we can choose it to be either isotropic or with block-diagonal constitutive tensors such that $\boldsymbol{\epsilon}_{st} = \boldsymbol{\epsilon}_{ts} = 0$ and $\boldsymbol{\mu}_{st} = \boldsymbol{\mu}_{ts} = 0$ (note that these last conditions are verified for reciprocal waveguide [26]). As a trivial consequence, in this case both matrices $\mathbf{T}$ and $\mathbf{S}$, defined in (7) and (10), become identity matrices. If we also assume that the perturbations are small, i.e., $\boldsymbol{\epsilon} \approx \bar{\boldsymbol{\epsilon}}$ and $\boldsymbol{\mu} \approx \bar{\boldsymbol{\mu}}$, then we can write $\mathbf{M}(s) \approx \boldsymbol{\epsilon} - \bar{\boldsymbol{\epsilon}}$ and $\mathbf{N}(s) \approx \boldsymbol{\mu} - \bar{\boldsymbol{\mu}}$. Eventually, these expressions allow us to simplify the coefficients $K_{\xi,\nu}^{(q,p)}$ and $C_{\xi,\nu}^{(q,p)}(s)$ to (12) and (13), respectively. For example, to achieve the approximation for $\mathbf{M}(s)$, we use the fact that the perturbation is small to approximate $\bar{\epsilon}_{ss}/\epsilon_{ss} \approx 1$ and to neglect terms of (8) that are of second order with respect to the perturbation $\boldsymbol{\epsilon} - \bar{\boldsymbol{\epsilon}}$. An analogous argument leads to the simplified form of $\mathbf{N}(s)$.

Another particular condition is when both the reference and the equivalent waveguide are isotropic. Direct calculations show that in this case the coupling coefficients simplify to:

$$K_{\xi,\nu}^{(q,p)} = \omega \iint (\epsilon - \bar{\epsilon}) \left(\mathbf{e}_{\xi t}^{(q)\top} \mathbf{e}_{\nu t}^{(p)} + \frac{\bar{\epsilon}}{\epsilon} \mathbf{e}_{\xi s}^{(q)\top} \mathbf{e}_{\nu s}^{(p)} \right) \mathrm{d}A, \tag{45}$$

$$C_{\xi,\nu}^{(q,p)} = -\omega \iint (\mu - \bar{\mu}) \left(\mathbf{h}_{\xi t}^{(q)\top} \mathbf{h}_{\nu t}^{(p)} + \frac{\bar{\mu}}{\mu} \mathbf{e}_{\xi s}^{(q)\top} \mathbf{e}_{\nu s}^{(p)} \right) \mathrm{d}A, \tag{46}$$

where the expression of $K_{\xi,\nu}^{(q,p)}$ is equivalent to that proposed in Ref. [14]. It must be remarked, however, that while having an isotropic reference waveguide is, as already noted, just a matter of choice, having an isotropic equivalent waveguide requires peculiar conditions to be verified. Specifically, according to the general expressions (2), the equivalent waveguide is isotropic if and only if the constitutive tensors of the real waveguide can be expressed as $\tilde{\boldsymbol{\epsilon}} = \epsilon\,(\det \boldsymbol{J}_{\boldsymbol{\sigma}})(\boldsymbol{J}_{\boldsymbol{\sigma}}^{\top}\boldsymbol{J}_{\boldsymbol{\sigma}})^{-1}$ and $\tilde{\boldsymbol{\mu}} = \mu\,(\det \boldsymbol{J}_{\boldsymbol{\sigma}})(\boldsymbol{J}_{\boldsymbol{\sigma}}^{\top}\boldsymbol{J}_{\boldsymbol{\sigma}})^{-1}$, where ϵ and μ are the scalar permittivity and permeability of the equivalent waveguide. Nevertheless these equations can be verified only when the real waveguide is isotropic and the transformation $\boldsymbol{\sigma}$ is such that $\boldsymbol{J}_{\boldsymbol{\sigma}}^{\top}\boldsymbol{J}_{\boldsymbol{\sigma}} = \boldsymbol{I}$. This means that the Jacobian matrix of $\boldsymbol{\sigma}$ must be orthogonal, which occurs, however, only when $\boldsymbol{\sigma}$ is a conformal map, that is, a transformation that preserves the local angles. For completeness, we note that when the real waveguide is anisotropic, the above equations are verified only if the constitutive tensors are proportional to each other and the geometric transformation $\boldsymbol{\sigma}$ is strictly mathematically related to the anisotropy; indeed a rather unrealistic case.

REFERENCES

[1] D. J. Richardson, J. M. Fini, and L. E. Nelson, "Space-division multiplexing in optical fibres," *Nature Photonics*, vol. 7, no. 5, pp. 354–362, May 2013.

[2] M. Notomi, A. Shinya, S. Mitsugi, E. Kuramochi, and H.-Y. Ryu, "Waveguides, resonators and their coupled elements in photonic crystal slabs," *Opt. Express*, vol. 12, no. 8, pp. 1551–1561, Apr. 2004.

[3] A. W. Snyder and Love, J., *Optical Waveguide Theory*, ser. Science Paperbacks. Springer, 1983.

[4] R. J. Black and L. Gagnon, *Optical Waveguide Modes: Polarization, Coupling and Symmetry*. McGraw-Hill Education, 2010.

[5] O. C. Zienkiewicz, R. L. Taylor, and J. Z. Zhu, *The finite element method: its basis and fundamentals*. Elsevier, 2005.

[6] J.-F. Lee, D.-K. Sun, and Z. Cendes, "Full-wave analysis of dielectric waveguides using tangential vector finite elements," *IEEE Transactions on Microwave Theory and Techniques*, vol. 39, no. 8, pp. 1262–1271, 1991.

[7] H. P. Uranus and H. J. W. M. Hoekstra, "Modelling of microstructured waveguides using a finite-element-based vectorial mode solver with transparent boundary conditions," *Opt. Express*, vol. 12, no. 12, p. 2795, 2004.

[8] M. Sodha and A. Ghatak, *Inhomogeneous Optical Waveguides*, ser. Optical Physics and Engineering. Springer, 1977.

[9] A. Yariv, "On the coupling coefficients in the coupled-mode theory," *Proc. IRE*, vol. 46, no. 12, pp. 1956–1957, Dec. 1958.

[10] D. Marcuse, "Coupled-mode theory for anisotropic optical waveguides," *Bell Labs Tech. J.*, vol. 54, no. 6, pp. 985–995, Jul. 1975.

[11] W.-P. Huang, "Coupled-mode theory for optical waveguides: an overview," *J. Opt. Soc. Am. A*, vol. 11, no. 3, pp. 963–983, Mar. 1994.

[12] H. Haus, W. Huang, S. Kawakami, and N. Whitaker, "Coupled-mode theory of optical waveguides," *J. Light. Technol.*, vol. 5, no. 1, pp. 16–23, Jan. 1987.

[13] A. Hardy and W. Streifer, "Coupled mode theory of parallel waveguides," *J. Light. Technol.*, vol. 3, no. 5, pp. 1135–1146, Oct. 1985.

[14] W.-P. Huang and J. Mu, "Complex coupled-mode theory for optical waveguides," *Opt. Express*, vol. 17, no. 21, pp. 19 134–19 152, Oct. 2009.

[15] J. Xu and Y. Chen, "General coupled mode theory in non-Hermitian waveguides," *Opt. Express*, vol. 23, no. 17, pp. 22 619–22 627, Aug. 2015.

[16] W. Chen, Z. Xiong, J. Xu, and Y. Chen, "Generalized coupled-mode formalism in reciprocal waveguides with gain, loss, anisotropy, or bianisotropy," *Phys. Rev. B*, vol. 99, no. 19, p. 195307, May 2019.

[17] M. Skorobogatiy, S. A. Jacobs, S. G. Johnson, and Y. Fink, "Geometric variations in high index-contrast waveguides, coupled mode theory in curvilinear coordinates," *Opt. Express*, vol. 10, no. 21, pp. 1227–1243, Oct. 2002.

[18] M. Skorobogatiy, S. G. Johnson, S. A. Jacobs, and Y. Fink, "Dielectric profile variations in high-index-contrast waveguides, coupled mode theory, and perturbation expansions," *Phys. Rev. E*, vol. 67, no. 4, p. 046613, Apr. 2003.

[19] R. Ulrich and A. Simon, "Polarization optics of twisted single-mode fibers," *Appl. Opt.*, vol. 18, no. 13, pp. 2241–2251, Jul. 1979.

[20] L. Palmieri and A. Galtarossa, "Coupling Effects Among Degenerate Modes in Multimode Optical Fibers," *IEEE Photonics J.*, vol. 6, no. 6, pp. 1–8, Dec. 2014.

[21] L. Palmieri, "Coupling mechanism in multimode fibers," in *Next-Generation Optical Communication: Components, Sub-Systems, and Systems III*, vol. 9009, 2014.

[22] M. Lohmeyer, N. Bahlmann, and P. Hertel, "Geometry tolerance estimation for rectangular dielectric waveguide devices by means of perturbation theory," *Optics Communications*, vol. 163, no. 1, pp. 86–94, May 1999.

[23] G. Guerra, S. M. Abokhamis Mousavi, A. Taranta, E. N. Fokoua, M. Santagiustina, A. Galtarossa, F. Poletti, and L. Palmieri, "A novel approach to coupled-mode analysis of geometric deformations in reciprocal waveguides," in *2020 European Conference on Optical Communications (ECOC)*, 2020.

[24] J. B. Pendry, D. Schurig, and D. R. Smith, "Controlling electromagnetic fields," *Science*, vol. 312, no. 5781, pp. 1780–1782, 2006.

[25] A. J. Ward and J. B. Pendry, "Refraction and geometry in maxwell's equations," *J. Mod. Opt*, vol. 43, no. 4, pp. 773–793, 1996.

[26] C. G. Someda, *Electromagnetic Waves*. Crc Press, 2006.

[27] K. Shastri, M. I. Abdelrahman, and F. Monticone, "Nonreciprocal and Topological Plasmonics," *Photonics*, vol. 8, no. 4, p. 133, Apr. 2021.

[28] J. B. Pendry, D. Schurig, and D. R. Smith, "Controlling Electromagnetic Fields," *Science*, vol. 312, no. 5781, pp. 1780–1782, Jun. 2006.
[29] A. Nicolet, F. Zolla, Y. Ould Agha, and S. Guenneau, "Geometrical transformations and equivalent materials in computational electromagnetism," *COMPEL - The international journal for computation and mathematics in electrical and electronic engineering*, vol. 27, no. 4, pp. 806–819, Jan. 2008, publisher: Emerald Group Publishing Limited.
[30] G. Guerra, M. Lonardi, A. Galtarossa, L. A. Rusch, A. Bononi, and L. Palmieri, "Analysis of modal coupling due to birefringence and ellipticity in strongly guiding ring-core OAM fibers," *Opt. Express*, vol. 27, no. 6, pp. 8308–8326, Mar. 2019.
[31] A. Villeneuve, "Orthogonality Relationships for Waveguides and Cavities with Inhomogeneous Anisotropic Media," *IEEE Trans. Microw. Theory Tech.*, vol. 7, no. 4, pp. 441–446, Oct. 1959.
[32] P. McIsaac, "Mode orthogonality in reciprocal and nonreciprocal waveguides," *IEEE Trans. Microw. Theory Tech.*, vol. 39, no. 11, pp. 1808–1816, Nov. 1991.
[33] Z. Sacks, D. Kingsland, R. Lee, and Jin-Fa Lee, "A perfectly matched anisotropic absorber for use as an absorbing boundary condition," *IEEE Trans. Antennas Propagat.*, vol. 43, no. 12, pp. 1460–1463, Dec. 1995.
[34] J. Hu and C. R. Menyuk, "Understanding leaky modes: slab waveguide revisited," *Adv. Opt. Photon.*, vol. 1, no. 1, pp. 58–106, Jan. 2009.
[35] COMSOL Inc., "Comsol.". Available: www.comsol.com
[36] D. Chowdhury and D. Wilcox, "Comparison between optical fiber birefringence induced by stress anisotropy and geometric deformation," *IEEE J. Sel. Top. Quantum Electron.*, vol. 6, no. 2, pp. 227–232, Mar. 2000.
[37] L. Palmieri and A. Galtarossa, "Intramodal Dispersion Properties of Step-Index Few-Mode Spun Fibers," *J. Light. Technol.*, vol. 34, no. 2, pp. 303–313, 2016.
[38] R. T. Schermer and J. H. Cole, "Improved Bend Loss Formula Verified for Optical Fiber by Simulation and Experiment," *IEEE J. Quantum Electron.*, vol. 43, no. 10, pp. 899–909, 2007.
[39] M. Skorobogatiy, K. Saitoh, and M. Koshiba, "Full-vectorial coupled mode theory for the evaluation of macro-bending loss in multimode fibers. application to the hollow-core photonic bandgap fibers." *Opt. Express*, vol. 16, no. 19, pp. 14 945–14 953, Sep. 2008.
[40] R. Ulrich, S. C. Rashleigh, and W. Eickhoff, "Bending-induced birefringence in single-mode fibers," *Opt. Lett.*, vol. 5, no. 6, pp. 273–275, Jun. 1980.
[41] M. Napiorkowski and W. Urbanczyk, "Rigorous modeling of twisted anisotropic optical fibers with transformation optics formalism," *Opt. Express*, vol. 29, no. 10, pp. 15 199–15 216, May 2021.
[42] H. Sakr, Y. Chen, G. T. Jasion, T. D. Bradley, J. R. Hayes, H. C. H. Mulvad, I. A. Davidson, E. Numkam Fokoua, and F. Poletti, "Hollow core optical fibres with comparable attenuation to silica fibres between 600 and 1100 nm," *Nat. Commun*, vol. 11, no. 1, p. 6030, 2020.
[43] F. Poletti, "Nested antiresonant nodeless hollow core fiber," *Opt. Express*, vol. 22, no. 20, pp. 23 807–23 828, 2014.
[44] G. T. Jasion, T. D. Bradley, H. Sakr, J. R. Hayes, Y. Chen, A. Taranta, H. C. H. Mulvad, I. A. Davidson, N. V. Wheeler, E. R. Numkam Fokoua, W. Wang, D. J. Richardson, and F. Poletti, "Recent breakthroughs in hollow core fiber technology," in *Next-Generation Optical Communication: Components, Sub-Systems, and Systems IX*. San Francisco, United States: SPIE, 2020, p. 1.
[45] E. A. J. Marcatili and R. A. Schmeltzer, "Hollow Metallic and Dielectric Waveguides for Long Distance Optical Transmission and Lasers," *Bell Labs Tech. J.*, vol. 43, no. 4, pp. 1783–1809, Jul. 1964.

APPENDIX C
BIOGRAPHY SECTION

Gianluca Guerra received his M. Sc. Degree in Telecommunication Engineering in 2017 and his Ph.D. degree in Information Engineering in 2021 from the University of Padova (Italy). He is currently a post-doctoral researcher at the Optoelectronics Research Centre, University of Southampton (United Kingdom). His research interests include the theoretical and numerical modelling and the characterization of light's propagation in hollow-core antiresonant optical fibers and in fibers for space-division multiplexing transmissions.

Seyed Mohammad Abokhamis Mousavi received MSc. in electrical–electronics engineering from Amirkabir university of technology (2008) before moving to Southampton where he received MSc. and Ph.D. degrees from Optoelectronics Research Centre, Southampton, UK (2018). His Ph.D. research has focused on the design and modeling of new hollow core fibers and studying the nonlinear optical effects in the gas-filled hollow core fibers. In 2018, he started a new role as Research Fellow at Optoelectronics Research Centre, where his research focuses on the design and study of new hollow core fibers for sensing applications. His main interests included hollow core fibers for special applications (polarization maintaining, sensing application, modal control, etc), nonlinear optics (pulse compression, Raman generation in gas-filled fibers, soliton generation, etc.), coherent control on metamaterials, and quantum photonics (entangled photon generation).

Austin Taranta is a researcher in the Optoelectronics Research Centre (ORC) at the University of Southampton. He received a BSc. in Chemical Engineering from the Massachusetts Institute of Technology in 2006. From 2006 to 2016, he served as an Optical Engineer with Honeywell Aerospace in Phoenix, Arizona developing high-performance fiber optic gyroscopes for defence and space applications. In 2016, he joined the ORC where he researches novel specialty and micro-structured fibers for gyroscopes and sensing applications. His current areas of interest include modal and polarization guidance effects in hollow-core antiresonant optical fibers, absorption spectroscopy and analytical chemistry in hollow-core optical fibers, multi-core and specialty solid optical fibers for sensing applications, and application of novel fibers to interferometric and resonator fiber gyroscopes. He holds several patents and he has authored more than 30 peer-reviewed conference and journal publications.

Eric Numkam Fokoua *(Member, IEEE)* received the B.Sc. degree in microelectronics from Nankai University, Tianjin, China, in 2008, the M.Sc. degree in photonics from the Universities of St. Andrews, Scotland, and Ghent, Belgium, in 2010, and the Ph.D. degree in optoelectronics from the Optoelectronics Research Centre, Southampton, U.K., in 2014, for the work on the numerical modelling of hollow-core optical fibers. His research interests include theoretical and numerical modeling of optical waveguides, in particular microstructured optical fibers and their applications. He currently holds a Royal Academy of Engineering Research Fellowship and was the recipient of the Corning Outstanding Student Paper Award in 2012 and the Tingye Li Innovation Prize in 2019.

Marco Santagiustina *(Member, IEEE)* received the Ph.D. degree in telecommunication engineering from the University of Padova (Italy) in 1996. He was Fulbright Visiting Scholar at the Optical Sciences Center, University of Arizona in 1995, Visiting Research Lecturer at the University of New Mexico and Visiting Scholar at Brown University in 1996. From 1997 to 1999, he was Postdoctoral Researcher at the University of the Balearic Islands, Spain. Since 1999, he has been with the Department of Information Engineering, University of Padua, Padua, Italy (Research Fellow 1999-2010, Associate Professor 2011-2020, Full professor from 2021). His main research interests include nonlinear optics and optical communications. He is coauthor of more than 130 articles and memories published in international scientific reviews, books, and proceedings of international conferences. He was the Coordinator of the FP7, FET-Open Project GOSPEL.

Andrea Galtarossa *(Fellow, IEEE)* is a professor of electromagnetic fields at DEI, University of Padova, Italy. His research activity is dedicated to birefringence effects in single-mode fibers, distributed measurements of birefringence in optical fiber, design of optimized spun fibers, few mode fibers design and characterization, distributed optical fiber sensors. He has been a member of the TPC of ECOC and OFC; and the Technical Program Co-Chair for ECOC 2010. He has authored or co-authored more than 200 papers on international peer-review journals and in the proceedings of international conferences and inventor (or one of the inventors) of seven international patents. He has been the Topical Editor of OSA Optics Letters (2008-2013) and the Deputy Editor of the OSA Optics Letters (2014-2020). He is Fellow of OPTICA.

Francesco Poletti *(Senior Member, IEEE)* received the Laurea degree in electronics engineering from the University of Parma, Parma, Italy, in 2000, and the Ph.D. degree from the Optoelectronics Research Centre (ORC), University of Southampton, Southampton, U.K., in 2007. He is currently a Professor with ORC. He was with Marconi Communications for three years and worked on optical network design and for more than ten years on the development of new generations of microstructured optical fibers with the ORC. He has co-authored more than 100 journal and 300 conference publications, and produced 12 patents. His research interests include the design of photonic bandgap and antiresonant fibers, the development of fiber-optic characterization techniques, and the fabrication of nonsilica-based fibers and devices. He is the holder of a European Research Fellowship Consolidator Grant.

Luca Palmieri *(Member, IEEE)* received the Ph.D. in Electronic and Telecommunication Engineering in 2000 from the University of Padova, Italy, where he has been Assistant Professor from 2004 to 2015 and is Associate Professor since 2015. His research activity is mainly focused on linear and non-linear propagation effects—including polarization and mode-coupling—in single- and few-mode optical fibers, with applications to telecommunication, fiber characterization and optical fiber sensors. He is or has been TPC member for several international conferences, such as ECOC, OFC and OFS. He has co-authored more than 190 scientific publications and has been associate editor of the Journal of Optics and Laser Technology (Elsevier) and topical editor of Optics Letters (Optica). He is member of IEEE and Optica.